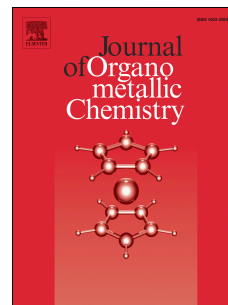


# Accepted Manuscript

Synthesis, structure, photophysical and electrochemical properties of Ru(TFA)(CO)(PPh<sub>3</sub>)<sub>2</sub>(L) (L=2-phenylpyridine, 2-*p*-tolylpyridine) and Ru(CO)(PPhMe<sub>2</sub>)<sub>2</sub>(L)(L') (L= TFA, H) (L'= bipyridine, L'= 4,4'-dimethylbipyridine) relationships between ancillary ligand structure and luminescent properties



Shyam Pohkrel, Dan Decato, Edward Rosenberg, J.B. Alexander Ross, Michelle Terwilliger

PII: S0022-328X(17)30174-2

DOI: [10.1016/j.jorganchem.2017.03.026](https://doi.org/10.1016/j.jorganchem.2017.03.026)

Reference: JOM 19860

To appear in: *Journal of Organometallic Chemistry*

Received Date: 15 November 2016

Revised Date: 9 March 2017

Accepted Date: 11 March 2017

Please cite this article as: S. Pohkrel, D. Decato, E. Rosenberg, J.B.A. Ross, M. Terwilliger, Synthesis, structure, photophysical and electrochemical properties of Ru(TFA)(CO)(PPh<sub>3</sub>)<sub>2</sub>(L) (L=2-phenylpyridine, 2-*p*-tolylpyridine) and Ru(CO)(PPhMe<sub>2</sub>)<sub>2</sub>(L)(L') (L= TFA, H) (L'= bipyridine, L'= 4,4'-dimethylbipyridine) relationships between ancillary ligand structure and luminescent properties, *Journal of Organometallic Chemistry* (2017), doi: 10.1016/j.jorganchem.2017.03.026.

This is a PDF file of an unedited manuscript that has been accepted for publication. As a service to our customers we are providing this early version of the manuscript. The manuscript will undergo copyediting, typesetting, and review of the resulting proof before it is published in its final form. Please note that during the production process errors may be discovered which could affect the content, and all legal disclaimers that apply to the journal pertain.



ACCEPTED MANUSCRIPT

Synthesis, structure, photophysical and electrochemical properties of  
Ru(TFA)(CO)(PPh<sub>3</sub>)<sub>2</sub>(L) (L=2-phenylpyridine, 2-*p*-tolylpyridine) and  
Ru(CO)(PPhMe<sub>2</sub>)<sub>2</sub>(L)(L') (L= TFA, H) (L' = bipyridine, L' = 4,4'-dimethylbipyridine)  
relationships between ancillary ligand structure and chemical properties<sup>‡</sup>

by

Shyam Pohkrel, Dan Decato, Edward Rosenberg,<sup>\*</sup> J. B. Alexander Ross and Michelle  
Terwilliger

Department of Chemistry and Biochemistry, University of Montana, Missoula, MT  
59812, USA

Corresponding Author: Edward Rosenberg, email: edward.rosenberg@mso.umt.edu

**Abstract**

The synthesis, structure and photophysical properties of the complexes  $[\text{Ru}[(\text{CO})(\text{TFA})(\text{PPh}_3)_2(\text{L})][(\text{L} = \text{ppy} = 2\text{-phenylpyridine, (1a); L} = 2\text{-(p-tolyl)pyridine} (\text{1b}), are reported. The complexes were characterized by UV-VIS, IR and NMR and by single-crystal X-ray diffraction techniques. We also report the synthesis, structure and photophysical properties of } [\text{Ru}(\text{CO})(\text{L})(\text{PPhMe}_2)_2(\text{L}')][\text{PF}_6]^- [\text{L}' = \text{bipyridine, L} = \text{TFA, (3a); L} = \text{H, (3b) and L} = \text{H, L}' = 4,4'\text{-dimethyl bipyridine (3c)}]. These compounds were characterized by UV-VIS, IR and NMR techniques and by a single crystal X-ray diffraction in the case of 3a. The solid state structure of } [\text{Ru}(\text{Me}_2\text{PhP})_2(\text{CO})_2(\text{TFA})_2 (\text{2}) which is the starting material for the synthesis 3a-3c is also reported to verify the *trans* relationship of the less bulky PPhMe<sub>2</sub> and for comparison with the previously reported PPh<sub>3</sub> analogs. The purpose of this study was to determine the impact, if any, of replacing bpy with ppy in the case of 1a and alkylation of the benzene ring in the case of 1b on the photophysical and electrochemical properties compared to related Ru(bpy) complexes. In contrast to the bpy analogs 1a and 1b showed reversible 1e<sup>-</sup> oxidations and blue-shifted MLCT absorptions. In the case of 3a-3c we were interested in the effect on the photophysical properties of substituting PPh<sub>3</sub> with the less bulky but more electron donating PPhMe<sub>2</sub>. There were only minor changes in the photophysical and electrochemical properties relative to the previously reported PPh<sub>3</sub> analogs.$

---

**Key words:** Ru complexes, phosphine ligands, bipyridine, 2-phenyl pyridine, photophysical properties, electrochemistry

## 1.0 Introduction

We have been studying the photophysical properties of ruthenium diimine complexes with a view towards developing probes for biomolecular dynamics with longer-lived excited states and higher quantum yields relative to the well-known Ru(tris-diimine)<sup>2+</sup> complexes [1,2]. Later, we immobilized the same complexes on solid surfaces and noted a large change in excited-state lifetime, an effect that could be useful in photo-promoted electron transfer chemistry [3]. The complexes of general formula [Ru(CO)(X)(L)(L')<sub>2</sub>]PF<sub>6</sub> (X = H, TFA)(L = bpy)(L' = PPh<sub>3</sub>) did exhibit the sought-after photophysical properties, having excited-state lifetimes in the neighborhood of 1 μs and quantum yields of 0.25 to 0.5. However, the complexes were only moderately stable in solution [4]. Measurements of the excitation spectra and time dependent density functional theory calculations indicates the phosphine ligand has a significant contribution to the excited state in these complexes [5]. With these observations in mind we decided to synthesize the 2-phenylpyridine (ppy) analogs of the bpy complexes and replaced the bulky PPh<sub>3</sub> with the smaller and more electron-donating PPhMe<sub>2</sub>. The ppy complexes of transition metals are more thermally stable than their bpy analogs due to the presence of one formally covalent bond and one coordinate covalent bond rather than the two coordinate covalent bonds formed with bpy [6]. The greater thermal stability of the ppy complexes has led to their extensive use in dye-sensitized solar cells [6e-6g]. Employing the less bulky PPhMe<sub>2</sub> could provide more surface mobility for the purported probe applications, however, the effect of a more electron-donating phosphine on the luminescent properties is unknown. We report here the synthesis,

structure, photophysical, and electrochemical properties of  $\text{Ru}[(\text{TFA})(\text{CO})(\text{PPh}_3)_2(\text{L})]$  ( $\text{L}=2\text{-phenylpyridine}$ , **1a**;  $2\text{-}p\text{-tolylpyridine}$ , **1b**) and  $\text{Ru}(\text{CO})(\text{PPhMe}_2)_2(\text{L})(\text{L}')$  ( $\text{L}=\text{TFA}$ ,  $\text{L}'=\text{bpy}$  **3a**;  $\text{L}=\text{H}$ ,  $\text{L}'=\text{bpy}$  **3b**;  $\text{L}=\text{H}$ ,  $\text{L}'=4,4'\text{-dimethylbipyridine}$ , **3c**) to understand the relationships between ancillary ligand structure and luminescent properties.

## 2.0 Experimental

### 2.1 Materials

Reactions were carried out using standard Schlenk line techniques under nitrogen unless otherwise noted. Column chromatography was performed using 60 Å pore size 230–400 mesh silica gel (Sorbent Technologies) and 58 Å pore size activated neutral alumina (Sigma–Aldrich). All solvents used such as ethylene glycol, dichloromethane and hexane used were reagent grade. Tetrahydrofuran (THF) was distilled from sodium benzophenone ketyl. Acetone and ethylene glycol were purchased from Fischer Scientific and VWR International, respectively. Ruthenium dodecacarbonyl, triphenylphosphine and dimethylphenylphosphine (Strem Chemicals) 2,2'-bipyridine, 4,4'-dimethyl-2,2'-bipyridine 2-phenylpyridine, 2-(*p*-tolyl)pyridine (Sigma–Aldrich) were used without further purifications. *N,N*-Diisopropylethylamine (DIPEA) was purchased from MP Biomedical LLC and Rhodamine–B needed for measurement of quantum yield was purchased from Sigma–Aldrich. The starting complexes  $\text{K}^+[\text{Ru}(\text{CO})_3(\text{TFA})_3]^-$  and  $\text{Ru}[(\text{CO})_2(\text{TFA})_2(\text{PPh}_3)_2]$  were synthesized according to literature procedures [1].

### 2.2 Methods

### 2.2.1 Spectroscopic Measurements

Solution NMR measurements were performed on a Bruker NMR systems spectrometer at 400 MHz, 376.55 MHz and 162 MHz for proton, fluorine and phosphorus, respectively and chemical shifts are reported relative to TMS ( $^1\text{H}$ ),  $\text{CFCl}_3$  ( $^{19}\text{F}$ ) and  $\text{H}_3\text{PO}_4$  ( $^{31}\text{P}$ ). IR spectra were recorded on a Nicolet iS7 and Thermo-Nicolet 633 FT-IR spectrometer as KBr pellets. Steady-state UV-Visible absorption and emission spectra were collected on Molecular Devices Spectra Max M2.

### 2.2.2 Excited-State Lifetime Measurements

Time-resolved luminescence decay measurements were performed by time correlated single-photon counting (TCSPC), using the Quantum Northwest FLASC 1000 sample Chamber (Spokane, WA). Pulsed excitation at 470 nm and a repetition rate of 50 KHz (external trigger) from a LDH-P-C 470 laser diode (PicoQuant, Berlin, Germany) were used to excite the complex for time-dependent studies. The luminescence decays were collected in the FLASC 1000 orthogonal to the excitation beam path at the magic angle polarization condition [7-8] using a 620/50 nm band pass filter (Chroma, Rockingham, VT, USA) to isolate the emissions and excitation scatter. All the measurements were taken at room temperature under normal atmospheric pressure. The decay curves were collected using the NanoHarp 250 PCI board (PicoQuant, Berlin) with a timing resolution of 560 ps/channel until  $4 \times 10^4$  counts at the peak were reached (see Supplementary Materials and Figure 1s) [9].

### 2.2.3. Solid State Structure of complexes

X-ray diffraction data for **1a**, **1b**, **2**, and **3a** were collected at 100 K on a Bruker D8 Venture using  $\text{MoK}\alpha$ -radiation ( $\lambda=0.71073 \text{ \AA}$ ). Data for **1a**, **1b** and **3a**

have been corrected for absorption using SADABS [11] area detector absorption correction program. Using Olex2 [12], the structures were solved with the ShelXT[13a] structure solution program using Direct Methods and refined with the ShelXL [13b] refinement package using least squares minimization. All non-hydrogen atoms were refined with anisotropic thermal parameters. Hydrogen atoms in the investigated structures were located from difference Fourier maps but finally their positions were determined geometrically, and refined with isotropic thermal parameters. Calculations and refinement of structures were carried out using APEX2 [14], SHELXTL [13c], and Olex2 software. Structure **2** was found to be a non-merohedral twin. The twin law found by Cell\_Now was -1.001 -0.001 0.000, 0.656 0.532 -0.471, -0.652 -1.524 -0.531 [13d]. Intensity data for **2** were integrated as two domains using SAINT [14b], and scaled with TWINABS [13e]. Refinement of HKLF5 data with ShelXL [13b] resulted in a BASF of 0.1129.

#### **2.2.4. Electrochemical measurements**

Half-wave potentials were measured on a BAS-100 electrochemical analyzer. Redox behavior of complexes was studied using a three-electrode standard cell with a glassy carbon electrode (diameter 0.1 cm sealed in epoxy resin) as the working electrode, an Ag/AgCl electrode as the reference and a platinum wire as the auxiliary electrode. Complexes ( $1 \times 10^{-3}$  M) were dissolved in dichloromethane containing 0.1 M  $[\text{NBu}_4^+\text{PF}_6^-]$  as the supporting electrolyte and the cell was deoxygenated with argon prior to each scan.

### **3.0 Synthesis**

### 3.1 Synthesis of Ru[(PPh<sub>3</sub>)<sub>2</sub>(CO)(TFA)(ppy-R)] (R=H, **1a**; R=Me, **1b**)

Ru[(PPh<sub>3</sub>)<sub>2</sub>(CO)<sub>2</sub>(TFA)<sub>2</sub>], [**1**] (100 mg, 0.109 mmol), was treated with 2-phenylpyridine (18.46 mg, 0.119 mmol) or 2-(p-tolyl)pyridine (20.19 mg, 0.119 mmol) in ethylene glycol (15 mL) and stirred for 72 h at 140 °C under nitrogen atmosphere. When the color of the reaction mixture turned to greenish-yellow, the reaction was cooled to room temperature and then filtered and washed three times with DI water to remove ethylene glycol. The solid was collected by centrifugation at 3000 rpm, washed 2× in DI water, followed by centrifugation, and then washed 1× with diethyl ether. Following the ether wash and rotary evaporation, the product was dissolved in a small amount of dichloromethane and then purified by neutral alumina column in a 1:1 mixture of hexane and dichloromethane as eluent. Two bands were observed and the slower greenish-yellow band was collected and solvent was removed by rotary evaporation followed by drying under high vacuum overnight. Greenish-yellow powders of Ru[(PPh<sub>3</sub>)<sub>2</sub>(CO)(TFA)(ppy)] (**1a**) (30mg, 29.57%) and Ru[(PPh<sub>3</sub>)<sub>2</sub>(CO)(TFA)(ppy-Me)] (**1b**) (35mg, 34 %) respectively were obtained. Elemental Analysis for **1a** calcd: C<sub>50</sub>H<sub>38</sub>F<sub>3</sub>NO<sub>3</sub>P<sub>2</sub>Ru: 65.21%, C; 4.16%, H; 1.52%, N; 6.73%, P. Found: 67.38%, C; 4.49%, %H; 1.80%, %N, 7.32% P. IR data for **1a** (as KBr pellets): 3047 (w) 1931(vs), 1684 (vs), 1433 (m), 695 (vs), 521 (vs) cm<sup>-1</sup>. NMR data for **1a**: (in CD<sub>2</sub>Cl<sub>2</sub>): <sup>1</sup>H, δ 6.73–8.78 (m, 38H); <sup>19</sup>F δ -75.39 (s), <sup>31</sup>P δ 33.50 (s). IR data for **1b** (as KBr pellets): 2900–3100, (w), 1931 (vs), 1685 (vs) 1433 (m), 695 (vs), 521 (vs) cm<sup>-1</sup>. NMR data for **1b** (in CD<sub>2</sub>Cl<sub>2</sub>): δ 6.56–8.78 (m, 37H), 1.93 (s, 3H); <sup>19</sup>F δ -75.27 (s); <sup>31</sup>P δ 34.10 (s).

### 3.2 Synthesis of Ru[(PPhMe<sub>2</sub>)<sub>2</sub>(CO)<sub>2</sub>(TFA)<sub>2</sub>] (2)

The ionic complex K<sup>+</sup>[Ru(CO)<sub>3</sub>(TFA)<sub>3</sub>]<sup>-</sup> (300 mg, 0.54 mmol) was refluxed with dimethyl phenyl phosphine (150 mg 1.08 mmol) in acetone solution for 24 h under a nitrogen atmosphere. Progress of the reaction was monitored by thin layer chromatography (TLC). After reaction the solvent was removed by rotary evaporation and the residue was dissolved in dichloromethane and chromatographed on a silica gel column. Elution with dichloromethane/acetone solution (98:2 v/v) gave two colorless bands. The faster moving band was collected and the solvent was removed by rotary evaporation and then dried overnight under high-vacuum. The product, **2**, was obtained (80 mg; 27%) as a shiny milky powder. **2**. IR (as KBr pellets): 2800–2950 (w), 2062 (vs), 2000 (vs), 1685 (vs), 1200 (vs) cm<sup>-1</sup>. <sup>1</sup>H NMR (in CDCl<sub>3</sub>): δ 7.47–7.52 (m, 10H), 1.74 (t, <sup>2</sup>J<sub>P-H</sub>=8 Hz, 12H); <sup>19</sup>F NMR: δ -74.16 (s); <sup>31</sup>P{<sup>1</sup>H} NMR: δ 4.8 (s).

### 3.3 Synthesis of [Ru(PPhMe<sub>2</sub>)<sub>2</sub>(CO)(X)(bpy-R)]<sup>+</sup>[PF<sub>6</sub>]<sup>-</sup> (**3a**, X = TFA, R=H), (**3b**, X = H R=H) and (**3c**, X = H, R=Me)).

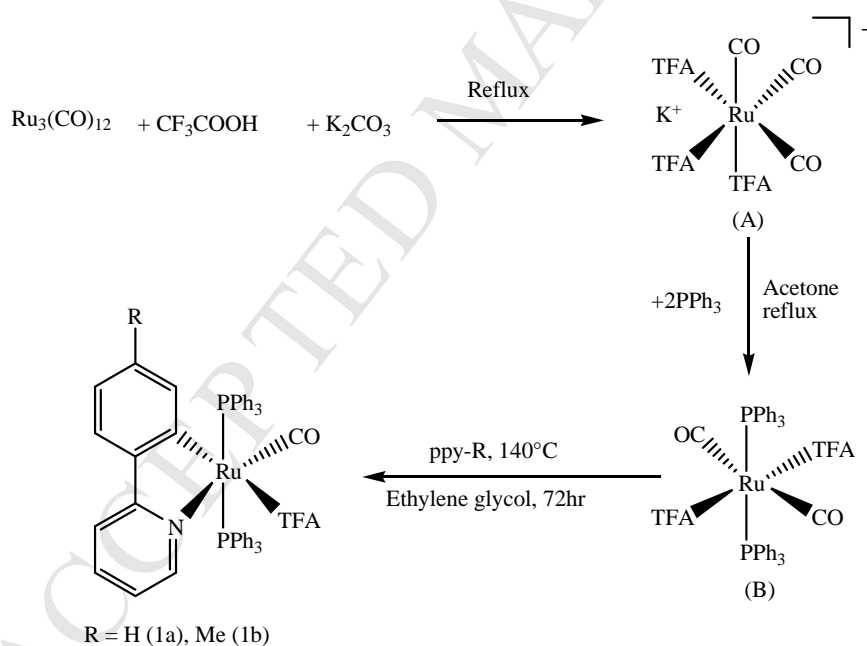
Reaction of complex **2** (100 mg, 0.15 mmol) with 2,2'-bipyridyl (25 mg, 0.15 mmol) in ethylene glycol (20 mL) at 140 °C for 72 h produced an orange colored solution of the cationic complexes of **3a** while the same reaction heated under the same conditions for 84 h with 2,2'-bipyridyl and 4,4'-dimethyl 2,2'-bipyridyl (28 mg, 0.15 mmol) gave a reddish-yellow solution of **3b** and **3c** respectively. Both solutions were treated with an aqueous solution of NH<sub>4</sub>PF<sub>6</sub> (concentration 1g/10 mL) dropwise until a precipitate was observed (6.5 mL). The resulting solution was refrigerated overnight to promote the complete precipitation, filtered and the

residue was washed several times with DI water to remove ethylene glycol, followed by centrifugation and finally washed with diethyl ether. The resulting product was dissolved in 5:2:2 hexanes/MeOH/CH<sub>2</sub>Cl<sub>2</sub> and then chromatographed using neutral alumina using the same solvent mixture as eluent which gave a single product band. Complete removal of solvent followed by drying under high vacuum overnight gave Ru[(PPhMe<sub>2</sub>)<sub>2</sub>(CO)(TFA)(2,2'-bpy)]<sup>+</sup>[PF<sub>6</sub>]<sup>-</sup> (40 mg, 28 %), (**3a**), [Ru(PPhMe<sub>2</sub>)<sub>2</sub>(CO)(2,2'-bpy)(H)]<sup>+</sup>[PF<sub>6</sub>]<sup>-</sup> (42mg, 34 %), (**3b**) and [Ru(PPhMe<sub>2</sub>)<sub>2</sub>(CO)(4,4-dimethyl-2,2'-bipyridyl)(H)]<sup>+</sup>[PF<sub>6</sub>]<sup>-</sup> (38 mg, 29 %), **3c**. IR data for **3a**: (as KBr pellets): 3055–2850 (w), 1970 (vs), 1680 (s) 840 cm<sup>-1</sup> (vs) cm<sup>-1</sup>. NMR data for **3a** (CDCl<sub>3</sub>): <sup>1</sup>H δ 6.66–8.51 (m, 18H), 1.56 (t, <sup>2</sup>J<sub>P-H</sub>=8.0 Hz, 6H), 1.52(t, <sup>2</sup>J<sub>P-H</sub>=8.0 Hz, 6H); <sup>19</sup>F NMR δ -71.78(d), -73.80(s); <sup>31</sup>P{<sup>1</sup>H} δ 3.37(s), -155 (sep). IR Data for **3b**: (as KBr pellets) 2850–2964 (w) 2028 (w), 1961 (vs), 838 (vs) cm<sup>-1</sup>. NMR data for **3b** (CDCl<sub>3</sub>): <sup>1</sup>H δ 6.66–8.23 (m, 18H), 1.50 (t, 6H, <sup>2</sup>J=8.0 Hz), 1.48(t, <sup>2</sup>J<sub>P-H</sub>=8.0 Hz, 6H), -12.36 (t, 1H, <sup>2</sup>J<sub>P-H</sub>=20); <sup>19</sup>F NMR ( -72.09, -73.98), <sup>31</sup>P{<sup>1</sup>H} δ 7.72 (s), -155(sep). IR Data for **3c**: (as KBr pellets): 2875 (w), 2077 (w), 1933 (vs), 908 (vs), 841 (vs), cm<sup>-1</sup>, NMR data for **3c** (CDCl<sub>3</sub>): δ 6.72–8.75 (m, 16H), 2.44 (s, 3H), -2.39 (s, 3H), 1.46 (t, <sup>2</sup>J<sub>P-H</sub>=8.0 Hz, 6H), 1.43 (t, <sup>2</sup>J<sub>P-H</sub>=8.0 Hz, 6H), -12.5 (t, 1H, <sup>2</sup>J<sub>P-H</sub>=20); <sup>19</sup>F NMR δ -73.95 (s), -71.98(d); <sup>31</sup>P{<sup>1</sup>H} NMR δ 8.23 (s), -155 (sep). Elemental Analysis for **3c**: calcd. for C<sub>29</sub>H<sub>34</sub>N<sub>2</sub>F<sub>6</sub>OP<sub>3</sub>Ru: C, 47.35%; H, 4.80%; N, 3.81%; P, 12.63%; found: C, 46.58%; H, 4.82%; N, 3.65%; P, 13.5%.

## 4.0 Results and Discussion

### 4.1 Synthesis and characterization of the 2-ppy complexes 1a and 1b

In our prior work on the synthesis of phosphine substituted diimine complexes of ruthenium we found that the anionic complex  $K^+[Ru(TFA)_3(CO)_3]^-$  is convenient starting material [1]. It is synthesized in high yield by refluxing  $Ru_3(CO)_{12}$  in trifluoroacetic acid followed by the addition of  $K_2CO_3$ . Although the starting material is much more expensive the resulting complex (intermediate A, Scheme 1) undergoes selective substitution with phosphines to give a *trans*-diphosphine as the only product under mild conditions (intermediate B scheme 1). Subsequent reaction with 2-ppy or 2-(*p*-tolylphenyl pyridine) to give  $[Ru(CO)(TFA)(PPh_3)_2(ppy-R)]$  (ppy=2-phenylpyridine (**1a**) and 2-(*p*-tolyl)pyridine (**1b**) respectively, by refluxing in ethylene glycol:



**Scheme 1.** Synthesis of **1a** and **1b**

Although there are numerous examples of ppy complexes in the literature [6] **1a** and **1b** are novel for Ru in containing two phosphines and a trifluoroacetate (TFA) ligand. They represent more thermally stable analogs of the recently reported bis-phosphine-bpy

analogs [6]. Thermal stability could be an important factor in the applications of these complexes for photo-promoted electron transfer.

The spectroscopic data for **1a** and **1b** are consistent with the structure proposed in Scheme 1. Both show a single  $\nu_{\text{CO}}$  at  $1931\text{ cm}^{-1}$  and carbonyl stretch at  $1685\text{ cm}^{-1}$  assigned to the TFA ligand, in addition to the expected bands in hydrocarbon and fingerprint region. The proton NMR of **1a** shows the expected aromatic resonances as does **1b** which also shows the tolyl methyl group at  $\delta$  1.93. Both compounds show nearly identical singlet resonances in the  $^{19}\text{F}$  ( $\delta$  -75.39 and -75.27 respectively) and  $^{31}\text{P}$  NMR ( $\delta$  33.50 and 34.10 respectively). Curiously, the elemental analysis for **1a** is in good agreement with the calculated % for H, N and P but gives a %C that is 2% higher than the calculated value. We attribute this to adsorbed solvent.

Single-crystal X-ray diffraction studies confirmed the structures of both **1a** and **1b**. Figures 1 and 2 show their solid-state structures. Relevant bond lengths and bond angles are given in the figure captions and crystal data is given in Table 1.

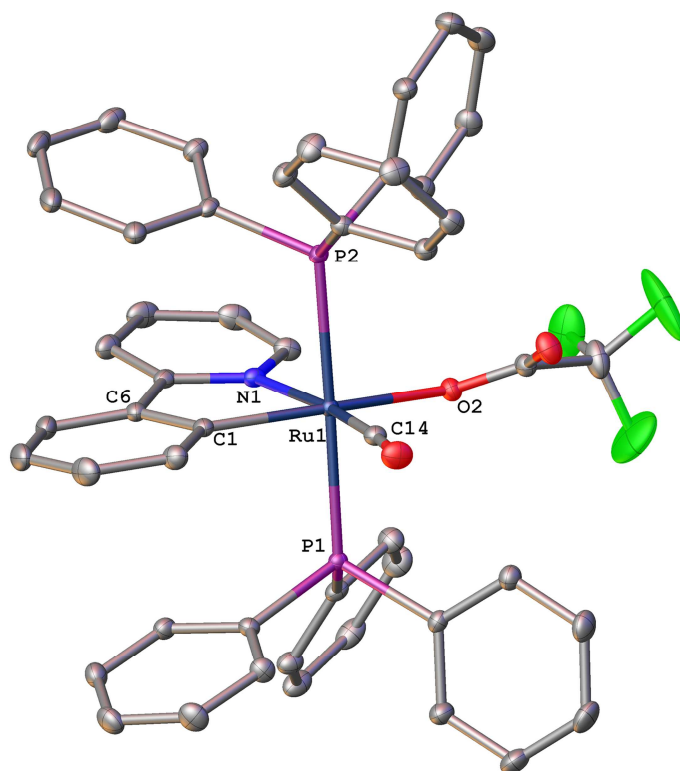


**Figure 1.** Solid-state structure of **1a** showing the 50% probability ellipsoids. All hydrogen atoms have been omitted for clarity. Ru(1)-P(1)=2.3758(3), Ru(1)-P(2)=2.4108(3), Ru(1)-O(2)=2.1957(9), Ru(1)-N(1)=2.1528(11), Ru(1)-C(1)=2.0432(13), Ru(1)-C(14)=1.8457(13) Å; P(1)-Ru(1)-P(2)=178.807(12), O(2)-Ru(1)-P(1)=87.24(3), O(2)-Ru(1)-P(2)=93.95(3), N(1)-Ru-P(1)=92.35(3), C(14)-Ru(1)-C(1)=90.90(6), C(6)-C(1)-Ru(1)=114.93(9)°.

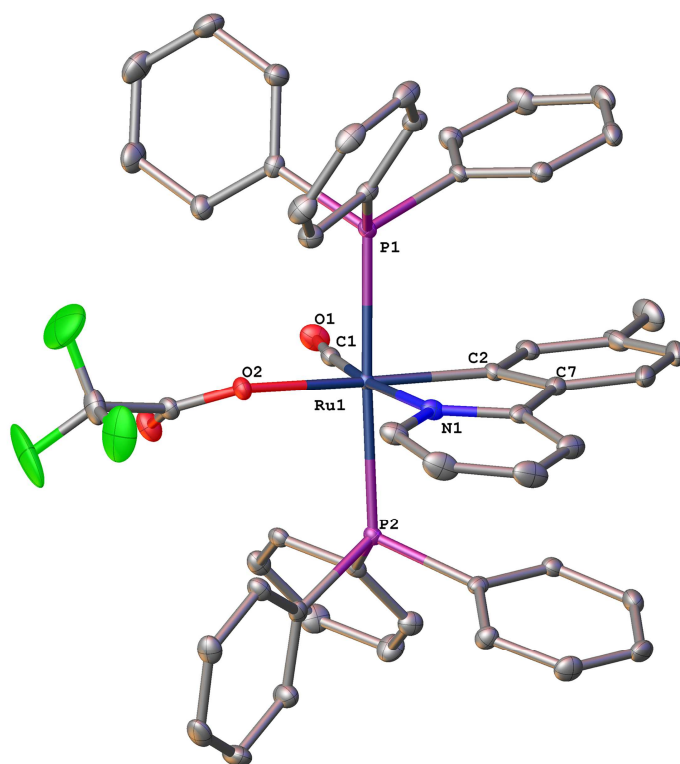


**Figure 2.** Solid-state structure of **1b** showing the 50% probability ellipsoids. All hydrogen atoms have been omitted for clarity. Ru(1)-P(1)=2.375(6), Ru(1)-P(2)=2.4200(6), Ru(1)-O(2)=2.2026(16), Ru(1)-N(1)=2.1541(18), Ru(1)-C(2)=2.036(2), Ru(1)-C(1)=1.848(2) Å; P(1)-Ru(1)-P(2)=177.37(2), O(2)-Ru(1)-P(1)=88.14(4), O(2)-Ru(1)-P(2)=94.50(4), N(1)-Ru-P(1)=93.04(5), C(1)-Ru(1)-C(2)=90.67(9), C(7)-C(2)-Ru(1)=115.09(16)°.

**Table 1.** Summary of crystal data and structure refinement for compound **1a**, **1b**, **2** and **3a**

Identification code	1a	1b	2	3a
Empirical formula	C <sub>50</sub> H <sub>38</sub> F <sub>3</sub> NO <sub>3</sub> P <sub>2</sub> Ru	C <sub>51</sub> H <sub>40</sub> F <sub>3</sub> NO <sub>3</sub> P <sub>2</sub> Ru	C <sub>22</sub> H <sub>22</sub> F <sub>6</sub> O <sub>6</sub> P <sub>2</sub> Ru	C <sub>29</sub> H <sub>30</sub> F <sub>9</sub> N <sub>2</sub> O <sub>3</sub> P <sub>3</sub> Ru
Formula weight	920.82	934.85	659.40	819.53
Temperature/K	100	100	100	100
Crystal system	monoclinic	monoclinic	triclinic	monoclinic
Space group	<i>P2</i> <sub>1</sub> / <i>c</i>	<i>P2</i> <sub>1</sub> / <i>c</i>	<i>P</i> -1	<i>Pn</i>
<i>a</i> /Å	11.5337(7)	11.6934(12)	9.3336(9)	9.3528(6)
<i>b</i> /Å	17.7170(10)	17.5395(18)	10.5722(10)	14.9723(10)
<i>c</i> /Å	20.5182(12)	20.976(2)	15.2426(14)	12.2752(8)
$\alpha$ /°	90	90	97.768(4)	90
$\beta$ /°	97.265(2)	94.796(3)	96.740(3)	111.739(2)
$\gamma$ /°	90	90	115.384(3)	90
Volume/Å <sup>3</sup>	4159.1(4)	4287.1(8)	1320.3(2)	1596.68(18)
<i>Z</i>	4	4	2	2
$\rho_{\text{calc}}$ /g/cm <sup>3</sup>	1.471	1.448	1.659	1.705
$\mu$ /mm <sup>-1</sup>	0.513	0.499	0.792	0.729
<i>F</i> (000)	1880.0	1912.0	660.0	824.0
Crystal size/mm <sup>3</sup>	0.25 × 0.25 × 0.15	0.2 × 0.15 × 0.1	0.4 × 0.4 × 0.3	0.2 × 0.15 × 0.15
Radiation	MoK $\alpha$ ( $\lambda$ = 0.71073)	MoK $\alpha$ ( $\lambda$ = 0.71073)	MoK $\alpha$ ( $\lambda$ = 0.71073)	MoK $\alpha$ ( $\lambda$ = 0.71073)
2 $\theta$ range for data collection/°	5.684 to 61.208	5.814 to 54.968	5.576 to 55.19	6.51 to 61.146
Index ranges	-16 ≤ <i>h</i> ≤ 16, -25 ≤ <i>k</i> ≤ 25, -29 ≤ <i>l</i> ≤ 29	-15 ≤ <i>h</i> ≤ 15, -22 ≤ <i>k</i> ≤ 22, -27 ≤ <i>l</i> ≤ 27	-12 ≤ <i>h</i> ≤ 11, -13 ≤ <i>k</i> ≤ 13, 0 ≤ <i>l</i> ≤ 19	-13 ≤ <i>h</i> ≤ 13, -21 ≤ <i>k</i> ≤ 21, -17 ≤ <i>l</i> ≤ 17
Reflections collected	243760	119854	6088	24363
Independent reflections	12796 [ <i>R</i> <sub>int</sub> = 0.0481, <i>R</i> <sub>sigma</sub> = 0.0186]	9824 [ <i>R</i> <sub>int</sub> = 0.1071, <i>R</i> <sub>sigma</sub> = 0.0395]	6088 [ <i>R</i> <sub>int</sub> = 0.0557, <i>R</i> <sub>sigma</sub> = 0.0391]	9732 [ <i>R</i> <sub>int</sub> = 0.0345, <i>R</i> <sub>sigma</sub> = 0.0501]
Data/restraints/parameters	12796/0/541	9824/0/551	6088/0/339	9732/2/428
Goodness-of-fit on <i>F</i> <sup>2</sup>	1.056	1.039	1.060	1.089
Final <i>R</i> indexes [ <i>I</i> ≥ 2 $\sigma$ ( <i>I</i> )]	<i>R</i> <sub>1</sub> = 0.0270, <i>wR</i> <sub>2</sub> = 0.0621	<i>R</i> <sub>1</sub> = 0.0392, <i>wR</i> <sub>2</sub> = 0.0954	<i>R</i> <sub>1</sub> = 0.0359, <i>wR</i> <sub>2</sub> = 0.0779	<i>R</i> <sub>1</sub> = 0.0388, <i>wR</i> <sub>2</sub> = 0.0775
Final <i>R</i> indexes [all data]	<i>R</i> <sub>1</sub> = 0.0354, <i>wR</i> <sub>2</sub> = 0.0661	<i>R</i> <sub>1</sub> = 0.0527, <i>wR</i> <sub>2</sub> = 0.1043	<i>R</i> <sub>1</sub> = 0.0479, <i>wR</i> <sub>2</sub> = 0.0832	<i>R</i> <sub>1</sub> = 0.0521, <i>wR</i> <sub>2</sub> = 0.0831
Largest diff. peak/hole / e Å <sup>-3</sup>	0.78/-0.50	2.01/-1.18	1.06/-0.56	1.18/-0.85

Crystals of **1a** and **1b** were grown by slow evaporation of a concentrated chloroform solution under a layer of pentane at room temperature. Both complexes crystallize in the monoclinic space group, *P2*<sub>1</sub>/*c* with four molecules in the unit cell.

The complexes **1a** and **1b** display distorted octahedral geometry where ppy-H or ppy-Me along with the carbonyl and TFA groups occupy a plane approximately perpendicular to the two *trans*-triphenylphosphine ligands. The P(1)–Ru–P(2) bond

angles for **1a** and **1b** are  $178.8^\circ(12)$  and  $177.37^\circ(2)$  (close to  $180^\circ$ ) respectively. These angles are very similar to those in the osmium analog of **1a**, which exhibits a P–Ru–P angle of  $176.78(6)^\circ$  [15]. The average Ru–P distances are  $2.392 \text{ \AA}$  for **1a** and  $2.397 \text{ \AA}$  for **1b**. These values are similar to those found in related octahedral iridium complexes where the average bond distance between central metal and phosphorous atom is  $2.390 \text{ \AA}$  [16]. As expected the Ru(1)–C(1) bond length in complex **1a** and the Ru(1)–C(2) in **1b**, are relatively shorter than the corresponding Ru–N bond distances in these complexes as well as in the related bpy complexes [1,17]. The formally anionic C(1) and C(2) are expected to be stronger  $\sigma$  donors than the nitrogen atoms in the ppy or bpy complexes. This results in an elongation of the Ru(1)–O(2) in **1a** ( $2.195 \text{ \AA}$ ) and the Ru(1)–O(2) in **1b** ( $2.201 \text{ \AA}$ ) being significantly longer than the Ru–O bonds in closely related Ru–TFA complexes ( $2.086$  to  $2.148 \text{ \AA}$ ) [where the Ru–O bond is trans to N and P respectively {1,17}]. A shorter Ru–O bond is also seen in **3a** relative to the same bonds in **1a** and **1b** (*vide infra*). This differential bond distance can be explained in terms of *trans*–effect of the coordinating groups. In both complexes the TFA and CO groups are *cis*- to each other with C(14)–Ru(1)–O(2) and C(1)–Ru(1)–O(2)  $102(5)^\circ$  and  $112.12(8)^\circ$  respectively. The presence of methyl group in **1b** increases the electron donating ability of the phenyl carbon to the metal center that causes a shortening of Ru(1)–C(11) ( $2.036(2) \text{ \AA}$ ) bond in **1b** relative to Ru(1)–C(1) ( $2.043(12) \text{ \AA}$ ) bond in **1a**.

#### 4.2 Synthesis and characterization of $[\text{Ru}(\text{PPhMe}_2)_2(\text{CO})_2(\text{TFA})_2]$ (**2**) and $[\text{Ru}(\text{PPhMe}_2)_2(\text{CO})\text{X}(\text{bpy-R})(\text{L}')^+][\text{PF}_6]^-$ (**3a-3c**)

In our prior work with the series of *bis*-phosphine ruthenium diimine complexes we focused on the  $\text{PPh}_3$  and the 1,2-diphenylphosphinoethene (dppene) ligands [1]. To

understand the relationship between phosphine bulkiness, electron donor ability and emission frequency we decided to synthesize PPhMe<sub>2</sub> analogs of the previously reported complexes. The first step involved the synthesis of the previously unknown precursor Ru(PPhMe<sub>2</sub>)<sub>2</sub>(CO)<sub>2</sub>(TFA)<sub>2</sub> (**2**). Refluxing the ionic complex K<sup>+</sup>[Ru(CO)<sub>3</sub>(TFA)<sub>3</sub>]<sup>-</sup> with PPhMe<sub>2</sub> in acetone solution for 24 h under a nitrogen atmosphere gave **2** in 27% yield. The IR showed the expected two νCO at 2062 and 2000 cm<sup>-1</sup> and a carbonyl stretch for the TFA ligand at 1685 cm<sup>-1</sup>. The <sup>19</sup>F NMR showed a singlet δ -74.16 and the <sup>31</sup>P{<sup>1</sup>H} NMR showed a singlet at δ 4.8. Interestingly, in addition to the expected phenyl resonances at δ 7.5 the methyl protons appeared as a 1:2:1 triplet instead of the expected doublet (Figure 3). We attribute this to the presence of a large <sup>31</sup>P-<sup>31</sup>P coupling that results in a virtual coupling as if the methyl groups were coupled to two equivalent phosphine ligands. This phenomenon is well documented in the literature and is common in complexes containing two *trans*-phosphine ligands [18] and in some cases with *cis*-phosphine ligands as well [19]. The outer wings of the triplet are taken as the value of the <sup>2</sup>J<sub>P-H</sub> for the doublet expected in the absence of virtual coupling, 8 Hz in the case of **2**.

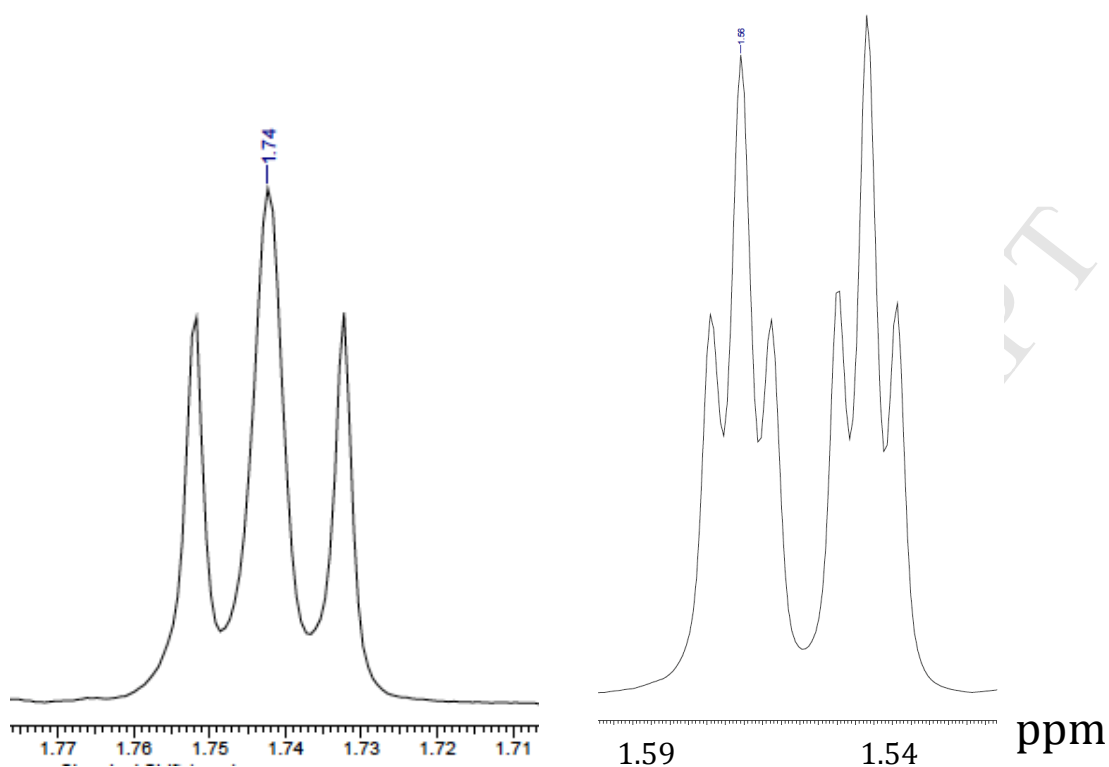


**Figure 3.** Methyl region of complex **2** (left); methyl region of complex **3a** (right)

To verify the proposed structure and the purported virtual coupling we undertook a single-crystal X ray-diffraction study of **2**. The solid-state structure of **2** is shown in Figure 4, with relevant bond length and angles are given in the figure caption and crystal data is given in Table 1. Complex **2** exists as an octahedral molecule with the two phosphine ligands in an almost perfect *trans*-position ( $P(1)-Ru-P(2)=176.30(3)^{\circ}$ ). The almost linear relationship between the two phosphorous atoms is consistent with strong  $^{31}P-^{31}P$  coupling that gives rise to the observed virtual coupling. The two carbonyl groups and the two TFA groups are *cis*- to each other as one would expect based on the strong  $\pi$ -acceptor properties of CO. All of the bond angles between the neighboring ligands are close to  $90^{\circ}$  except the  $O(3)-Ru(1)-O(5)$  angle which is  $79.64(8)^{\circ}$ . The two carbonyl oxygen atoms of the TFA

groups point away from each other and the contraction in the bond angle could be the result of steric effect with the neighboring CO ligands. The Ru-P bonds are only slightly different than the same bonds in complexes **1a** and **1b**.

ACCEPTED MANUSCRIPT

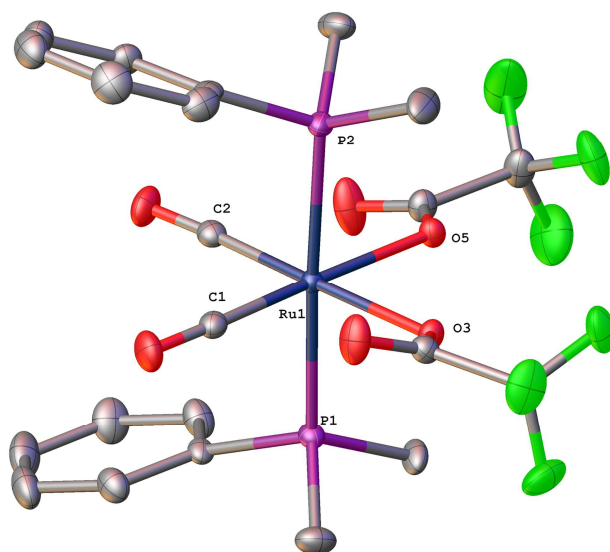
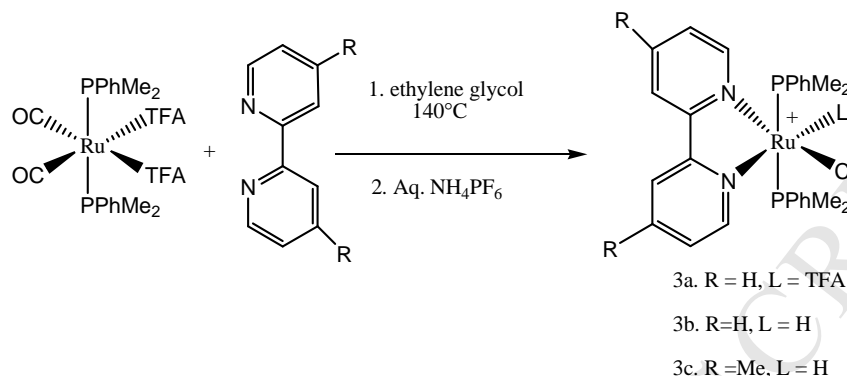


**Figure 4.** Solid-state structure of **2** showing the 50% probability ellipsoids. All hydrogen atoms have been omitted for clarity. Ru(1)-P(1)=2.3810(8), Ru(1)-P(2)=2.3790(8), Ru(1)-O(3)=2.103(2), Ru(1)-O(5)=2.0968(19), Ru(1)-C(1)=1.862(3), Ru(1)-C(2)=1.875(3) Å, P(1)-Ru(1)-P(2)=176.30(3), O(3)-Ru(1)-P(1)=87.60(6), O(3)-Ru(1)-P(2)=92.17(6), O(3)-Ru(1)-O(5)=79.64(8)<sup>o</sup>.

Refluxing **2** and bpy in ethylene glycol followed by addition of NH<sub>4</sub>PF<sub>6</sub> gave [Ru(CO)(bpy)(PPhMe<sub>2</sub>)<sub>2</sub>(TFA)]<sup>+</sup>[PF<sub>6</sub>]<sup>-</sup> (**3a**) (Scheme 2) in 28.2% yield. The IR spectroscopic data of **3a** shows the expected  $\nu_{\text{CO}}$  at 1970 cm<sup>-1</sup> and a carbonyl stretch from the TFA ligand at 1680 cm<sup>-1</sup>. The proton NMR shows the expected aromatic resonances at  $\delta$  6.66 – 8.51. As for **2**, virtual coupling is observed for the methyl resonances of the PPhMe<sub>2</sub> ligands where two triplets are observed at  $\delta$  1.52 and 1.56 (<sup>2</sup>J<sub>P-H</sub> = 8 Hz for both). The two triplets arise from the fact that in **3a** the methyl groups are diastereotopic due to the lack of symmetry in the plane perpendicular to the purported two mutually *trans*-phosphine ligands. Although the spectroscopic data is consistent with

the proposed structure a solid-state structural investigation was undertaken to verify our interpretation of the NMR data.



**Scheme 2.** Synthesis of **3a-3c** starting with **2**.

The solid-state structure of **3a** is shown in Figure 5, relevant bond distances and angles are given the figure caption and crystal data is given in Table 1.

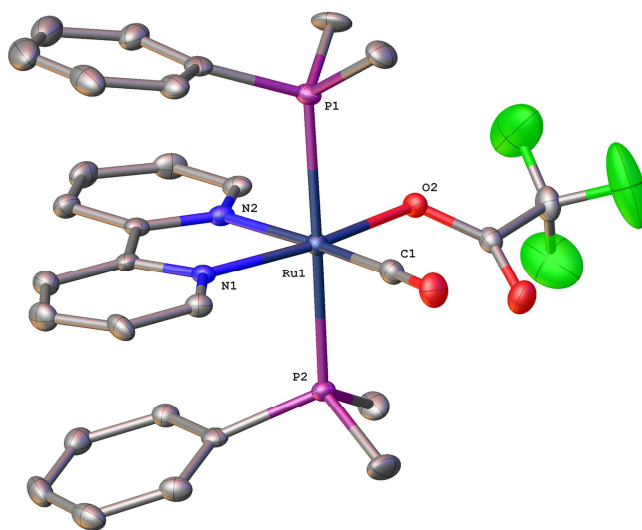


**Figure 5.** Solid-state structure of (**3a**) showing the 50% probability ellipsoids. All hydrogen atoms and the  $\text{PF}_6^-$  anion have been omitted for clarity. Ru(1)-P(1)=2.3755(12), Ru(1)-P(2)=2.3785(12), Ru(1)-O(2)=2.089(3), Ru(1)-N(1)=2.053(4), Ru(2)-N(2)=2.102(4), Ru(1)-C(1)=1.868(5) Å. P(1)-Ru(1)-P(2)=175.49(6), O(2)-Ru(1)-

N(2)=89.71(14), C(1)-Ru(1)-N(1)=95.22(18), N(1)-Ru(1)-N(2)=78.61(15), C(1)-Ru(1)-O(2)=96.46(18)<sup>o</sup>.

The solid-state structure of **3a** is that predicted from the NMR data. The two *trans*-phosphine ligands are perpendicular to the plane of the bpy, CO and TFA ligands and the bond lengths are similar to complexes **1a**, **1b**, **2** and related PPh<sub>3</sub> complexes [1]. The bond angles are close to the expected 90<sup>o</sup> with the exception of the N(1)-Ru(1)-N(2) (78.61(15)<sup>o</sup>) where the constraints of the bpy ligand geometry result in this smaller angle. Interestingly, the solid state structure of **3a** shows the phenyl groups of the PPhMe<sub>2</sub> lying directly over the bpy ring with the two phosphine ligands are in an eclipsed conformation with respect to each other. The distances between the centroids of the phenyl groups of the PPhMe<sub>2</sub> ligands and one of the aromatic rings of the bpy are 3.603(3) and 3.758(2) Å suggesting  $\pi$ -stacking interactions (Figure 6). However, the distances to the other bpy ring are significantly longer, being 4.471(3) and 4.284(3) Å. Although we cannot exclude the possibility that the observed ligand conformations are the result of crystal packing considerations the fact that the distances are shorter to one bpy ring supports the  $\pi$ -stacking argument. [20] (Figure 6). In crystal structures  $\pi$ -stacking interactions between aromatic or heteroaromatic rings range from 3.30 to 4.00 Å placing the observed values in the middle of this range for one of the two bpy rings and the phosphine phenyl ring in **3a** [20].

Heating complex **3a** in ethylene glycol leads to its conversion to the corresponding hydride, **3b**, a phenomenon that we previously observed in related Ru(bpy)(phosphine complexes) [1]. This is evident from the appearance of a triplet resonance at  $\delta$  -12.36 (t, 1H, <sup>2</sup>J<sub>P-H</sub>=20) and a weak band in the IR spectrum at 2028

$\text{cm}^{-1}$ . As for **3a** the phosphine methyl groups in **3b** appear as two triplets due to strong virtual  $^{31}\text{P}$ - $^{31}\text{P}$  coupling and the diastereomeric environment of the *trans*-phosphine ligands  $\delta$  1.50 (t, 6H,  $^2J=8.0$  Hz), 1.48(t,  $^2J\text{P-H}=8.0$  Hz, 6H).

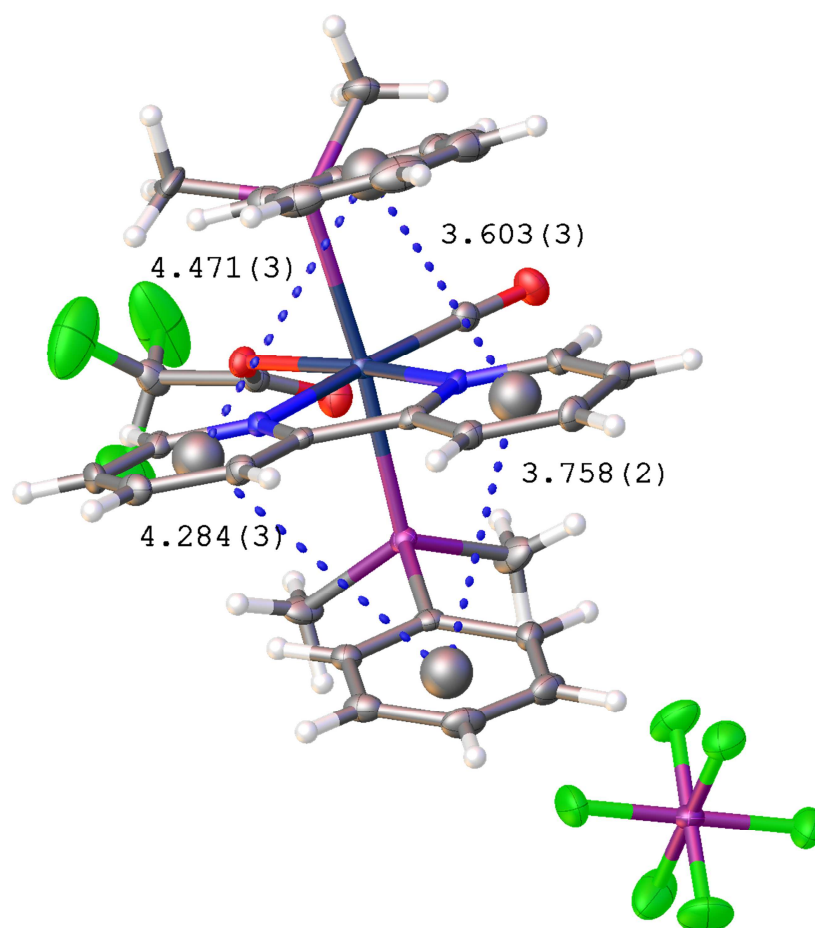


**Figure 6.** Complex **3a** showing the possible  $\pi$ - $\pi$  stacking of the phosphine phenyl and the bpy aromatic rings

A proposed target for the use of the Ru(bpy)(phosphine) complexes is to immobilize the complex on a surface to probe surface structure and its influence on photophysical properties [3]. In our previous studies we used peptide-coupling chemistry to bind the Ru complexes to the surface and poor loading was observed [2,3].

Functionalizing the bpy ring with a benzylic halide seemed like a promising alternative to a carboxylic acid and so we undertook the synthesis of a 4,4'-dimethyl-bpy derivative and thought it would be interesting to compare its photophysical and electrochemical properties with the unsubstituted bpy analogs, **3a** and **3b**.

Prolonged heating of complex **2** in the presence of 4,4'-bipyridine in ethylene glycol gave  $[\text{Ru}(\text{PPhMe}_2)_2(\text{CO})(\text{bpy-Me})(\text{H})]^+[\text{PF}_6]^-$  **3c** in 29.47% yield. Elemental analysis was in reasonable agreement with the formulation and the IR spectrum showed the expected frequencies for the hydride and the CO at 2077(w) and 1933(vs)  $\text{cm}^{-1}$  respectively. The proton NMR of **3c** shows two triplets at  $\delta$  1.46 (t,  $^2\text{J}_{\text{P-H}}=8.0$  Hz, 6H), 1.43 (t,  $^2\text{J}_{\text{P-H}}=8.0$  Hz, 6H), evidence for strong virtual  $^{31}\text{P}$ - $^{31}\text{P}$  coupling as observed for **2**, **3a** and **3b**. Two singlet resonances of each of relative intensity three are observed at  $\delta$  2.44 and 2.39 and are assigned to the methyl groups on the bpy ring which are magnetically nonequivalent by being *trans*- to either the hydride or the carbonyl groups. The hydride appears as a triplet at  $\delta$  -12.5 (1H,  $^2\text{J}_{\text{P-H}}=20$ ). The aromatic region at  $\delta$  6.72–8.75 integrates for 16 protons and resonances similar to **3a** and **3b** are observed in the  $^{31}\text{P}$  and  $^{19}\text{F}$  NMR. Based on these data **3c** is a direct structural analog of **3a** and **3b**.

#### 4.3 Electrochemical behavior of **1a**, **1b**, **3b** and **3c**

The redox properties of **1a**, **1b**, **3b** and **3c** were evaluated by cyclic voltammetry with Ag/AgCl as the reference electrode and 0.1M  $[\text{NBu}_4^+\text{PF}_6^-]$   $\text{CH}_2\text{Cl}_2$  solution as the electrolyte at a scan rate 50-100 mV/sec using a glassy carbon-working electrode. The complexes **1a** and **1b** exhibited quasi-reversible and reversible  $1e^-$ , metal-centered oxidation at +0.95 and +1.0 V respectively (Figure 7). The small shift to more positive

oxidation potential for **1b** cannot be attributed to the electron donating influence of the methyl group in the *trans*-position of the phenyl ring of the 2-ppy ligand as making the metal more electron rich would be expected to make the metal center more electron rich and easier to oxidize. This small difference could arise from changes in orbital energies at the metal center. The cathodic regions of **1a** and **1b** did not show any well-defined reductive waves and so are not included here

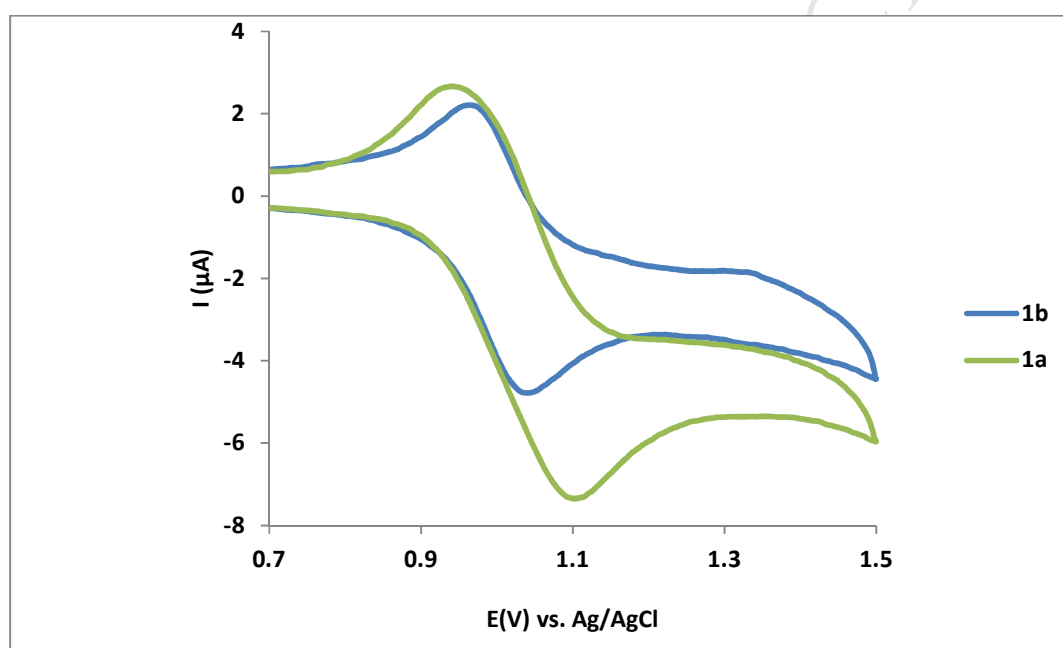


**Figure 7.** CV of a 1.0 mM solution of **1a** and **1b** in  $\text{CH}_2\text{Cl}_2$  containing 0.10  $\text{M}[\text{NBU}_4][\text{PF}_6]$ , at a glassy carbon working electrode

In the bipyridyl-based complexes, (**3b** and **3c**), the cyclic voltammetry responses are not well resolved and show a number of ill-defined peaks. Stabilization of a particular oxidation state is determined by the  $\sigma$ -donor and  $\pi$ -acceptor tendencies of surrounding ligands (Figure 8). The  $\sigma$  donor properties of ligands tend to stabilize Ru (III) over Ru (II) while the  $\pi$ -acceptor ligands lead to the stabilization of Ru (II) state.

For complex, **3b** two irreversible potential are observed at  $E^\circ = -1.3$  and  $E^\circ = -1.5$  V respectively versus Ag/AgCl. As expected the presence of the methyl groups *trans*- to the nitrogen atoms of the bpy ring in **3c** shifted the reduction potential to less negative values due to increased electron density at the metal and showed only one irreversible wave at -1.6V. No well-defined anodic waves were observed as for the previously reported bpy complexes [1]

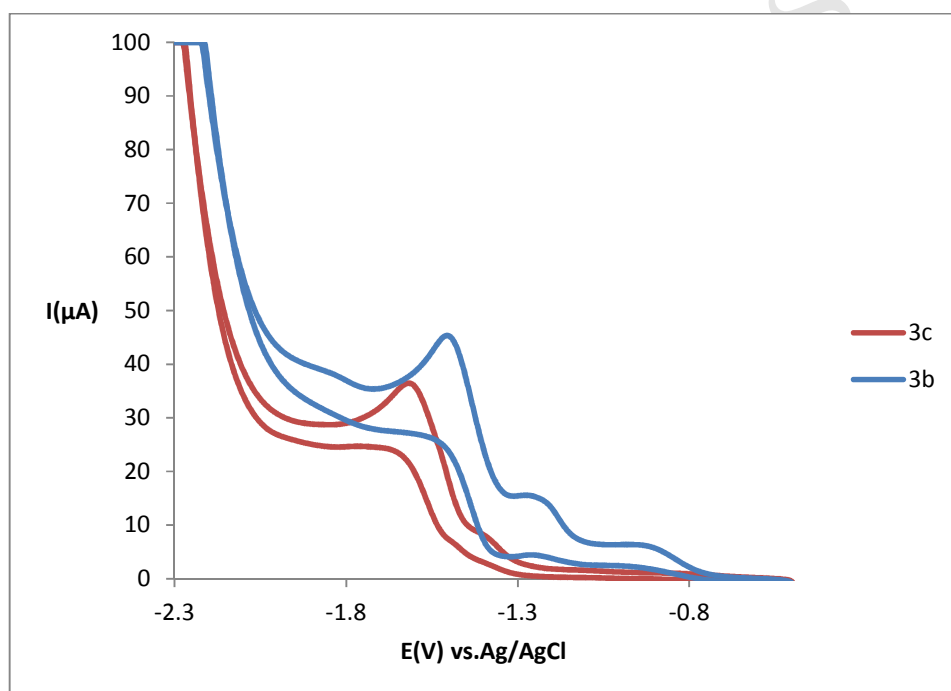


**Figure 8.** CV of a 1.0 mM solution of **3b** and **3c** in  $\text{CH}_2\text{Cl}_2$  containing 0.10  $\text{M}[\text{NBu}_4][\text{PF}_6]$ , at a glassy carbon working electrode

This general trend of irreversible multiple reduction potentials was observed in the previously reported hydrido- $\text{PPh}_3$  analogs of **3b** and **3c** and the potentials observed were similar to that reported here suggesting that increasing the electron-donating

properties of the phosphine has only a minimal effect on reduction potentials at the metal and the bpy ligand [1].

#### 4.4. Photophysical properties of complexes

The photophysical properties of the complexes of **1a**, **1b**, **3b** and **3c** are summarized in Table 2. All the complexes show the expected MLCT transitions with the most significant difference being that between **1a** and **1b** compared with **3b** and **3c**. The MLCT is significantly blue-shifted 80-90 nm in **1a** and **1b** with respect to **3b** and **3c**.

**Table 2.** UV–Vis absorption and emission data in CH<sub>2</sub>Cl<sub>2</sub>

Compound	$\lambda_{\text{abs}}$ MLCT (nm)	$\lambda_{\text{exc}}$ (nm)	$\lambda_{\text{e}}$ (nm)	$\tau$ (ns)
<b>1a</b>	390	390	–	–
<b>1b</b>	400	400	–	–
<b>3b</b>	480	470	600	330
<b>3c</b>	480	470	610	270

There is a small but significant red shift in the MLCT **1b** and **3c** relative to **1a** and **3b** as a result of methyl substitution, again due to the better electron donation that increases the HOMO-LUMO gap. All the complexes show intense absorptions in the range of 300-350 nm due to the intraligand absorptions of the ppy and bpy ligands. In the case of **3c** tails of these absorptions obscured the MLCT band but irradiation at 470 nm did give an emission at 610nm. Measurement of the excitation spectrum, monitoring at 610 nm, clearly showed that the emission at 610 nm came

from a hidden MLCT band at 470 nm that is obscured by the tail of the shorter wavelength absorptions (Figure 9).

Compounds **1a** and **1b** showed no significant emissions when irradiated at the MLCT. This is likely due to the increase in the HOMO-LUMO gap resulting from the strong  $\sigma$ -donor properties of the carbon atom bound to Ru. This results in a blue shifted MLCT band that brings this transition into close proximity with intraligand transitions leading to high internal conversion and radiationless decay. We have seen this phenomenon in related bpy complexes that exhibit blue-shifted MLCT [2,17].

Complexes **3b** and **3c** on the other hand showed red shifted emissions of sufficient intensity to allow measurement of their excited-state lifetimes. Here, unlike the case of the absorption and emission spectra of the PPh<sub>3</sub> analogs, **3a** and **3b** show a significant difference in lifetime. Complexes **3b** and **3c** showed much shorter lifetimes being 330 and 270 ns respectively whereas the related hydrido-triphenyl phosphine complexes showed lifetimes in the 500-700 ns range [1-3]. The lifetime of the triplet state will depend upon spin-orbit coupling and environmental factors that contribute to non-radiative decay [7], but we can tentatively point out that the PPhMe<sub>2</sub> ligand would be expected to have a lesser ability to delocalize electron density in the excited-state relative to the PPh<sub>3</sub> analogs.

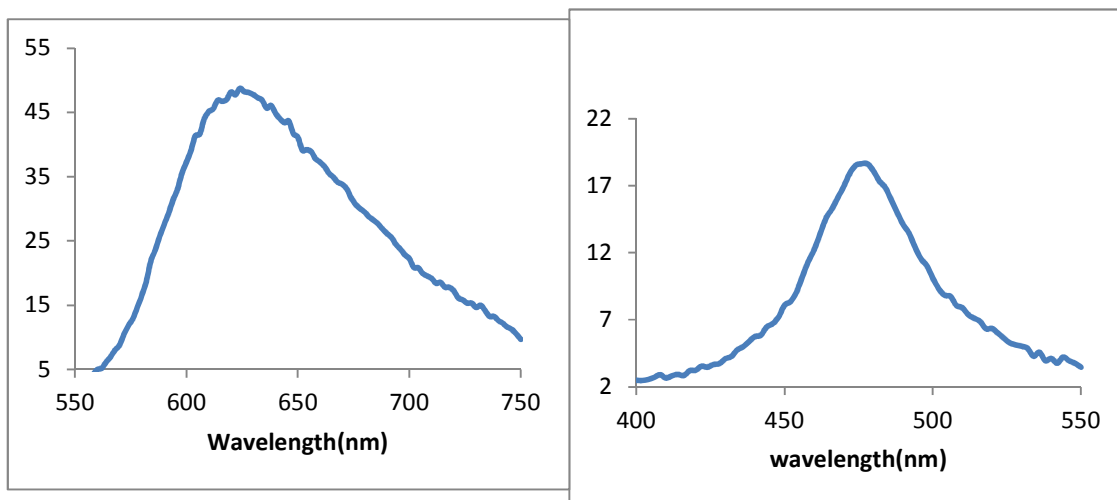


**Figure 9.** Emission (left) and excitation (right) spectra for **3c** measured in  $\text{CH}_2\text{Cl}_2$

## 5.0 Conclusions

The intent of this study was to compare the photophysical and electrochemical properties of related ppy and bpy complexes with a view towards developing them as probes of surface environments. Significant differences were noted, but not all of them suited our intended goals. The ppy ligands did not convert from their starting TFA derivatives to their corresponding hydride derivatives. The hydrides of ruthenium phosphine complexes are less likely to dissociate from the metal center than their TFA analogs in aqueous solution a property that is useful for the intended applications [1]. On the other hand the ppy complexes showed clean reversible  $1e^-$  oxidations while the bpy complexes showed multi-electron irreversible reductions and no well-defined oxidations [1]. The bpy ligands showed relatively intense emissions whose excited-state lifetimes could be measured while the ppy complexes were non-emissive. Perhaps most surprising was the similarity between the  $\text{PPhMe}_2$  and  $\text{PPh}_3$  complexes with regard to absorption and emission wavelengths. The less bulky nature of the  $\text{PPhMe}_2$  could still be useful for

studying surfaces but the hope was that its better electron donor properties would enhance emission intensity. In summary, the study has defined the limits of tunability for these two classes of bidentate ligands.

### Acknowledgements

The authors gratefully acknowledge the support of the National Science Foundation (CHE 1049569) for support of this research and for a grant to purchase a single crystal X-Ray diffractometer (CHE-MRI (CHE - 1337908)). We also acknowledge the NIH for support of the Biomolecular Structure and Dynamics Core facility at the University of Montana (CoBRE NIGMS P20GM103546). CCDC 1511195-1511198 contains the supplementary crystallographic data for **1a**, **1b**, **2**, and **3a**, respectively. These data can be obtained free of charge via a <http://www.ccdc.cam.ac.uk/conts/retrieving.html>, or from the Cambridge Crystallographic Data Centre, 12 Union Road, Cambridge CB2 1EZ, UK; fax: þ44 1223 336 033; or e-mail: [deposit@ccdc.cam.ac.uk](mailto:deposit@ccdc.cam.ac.uk).

‡ this paper is being submitted to the special issue of J. Organometal. Chem. in honor of Professor Richard D. Adam's 70<sup>th</sup> Birthday and in recognition of his outstanding research and service contributions to the inorganic/organometallic community

### References

1. A. Sharmin , R. C. Darlington , K. I. Hardcastle, M. Ravera, E. Rosenberg, J. B. A. Ross J. Organometal. Chem. 694 (2009) 988-1000.
2. A. Sharmin, L. Salassa, E. Rosenberg, J. B. A. Ross, G. Abbott, Geoffrey; L. Black, M. Terwilliger, R. Brooks, Inorg. Chem. 52 (2013) 10835-10845.
3. G. Abbott, R. Brooks, E. Rosenberg, M. Terwilliger, J. B. A. Ross and O. O. L. Ichire Organometallics 33 (2014) 2467 – 2478.

4. G. Abbott Doctoral Dissertation “ The Development and Study of Surface Bound Ruthenium Complexes,” University of Montana 2014.
5. S. Alabbad, E. Rosenberg, J. B. A. Ross, F. Ilu submitted.
6. a) C. D. Ertl, D. P. Ris, S. C. Meier, E. C. Constable, M. Neuberger, J. A. Zampese Dalton Trans. 44 (2015) 1557. b) M. Gruselle, R. Andres, B. Malezieux, C. Train, M. Verdaguer Chirality 13 (2001) 712. c) A. Hijazi, J.-P. Djukic, L. Allouche, A. de Cian, X.-F. Le Goff, L. Ricard Organometallics 26 (2007) 4180. d) M. Klajner, P. Hebraud, C. Sirlin, C. GaiddonS. Hariapp J. Phys. Chem. 114 (2010) 14041. e) Z. Ji, G. Natu, Y. Wu ACS Appl. Mater. Interfaces 5 (2013) 8641. f) P. Prompan, K. Wongkhan, R. Jichati Appl. Mater. Res. 770 (2013) 92. g) E. Yoneda, M. K. Nazeeruddin, M. Graetzel J. of Photopoly. Sci. and Tech.25, 25 (2012) 175.
7. C. A. Parker, Photoluminescence of Solutions with Application to Photochemistry and Analytical Chemistry, Elsevier, Amsterdam 1968, 262.
8. J. R. Lakowicz, Principles of Fluorescence Spectroscopy (3rd ed.) 2006, Springer, New York.
9. A.S. Minazzo, R.C. Darlington and J.B.A. Ross, Biophys. J. 96 (2009) 681.
10. M.L. Johnson and S.G. Frasier, In Methods Enzymol , Academic Press:, New York, 1985, 301.
11. G.M. Sheldrick, (2001), SADABS: Area Detector Absorption Correction, University of Gottingen, Germany.
12. O.V. Dolomanov, L.j. Gildea, J.A.K. Howard and S.Puschmann, J. Appl. Cryst., 42 (2009) 339
13. a) Sheldrick, G. M. (2015). Acta Cryst. A71, 3-8.0. b) Sheldrick, G. M. (2015). Acta Cryst. C71, 3-8. c) G.M. Sheldrick Acta. Cryst. 64 (2008) 112. d)

- Sheldrick, G. M. (2008). CELL\_NOW. Georg-August-Universität Göttingen, Göttingen, Germany. e) Sheldrick, G. M. (2012). TWINABS. Version Georg-August-Universität Göttingen, Göttingen, Germany.
14. a) Bruker (2007), APEX2, Bruker AXS Inc., Madison, Wisconsin, US. b) Bruker (2007). SAINT. Bruker AXS Inc., Madison, Wisconsin, USA.
15. A.M. Clark, C.E.F. Rickard, W.R. Roper and L.J.Wright, *Organometallics*, 18 (1999) 2813.
16. M.S. Eum, C.S. Chin, S.Y. Kim, C. Kim, S.K. Kang, N.H. Hur, J.H. Seo, G.Y. Kim and Y.K. Kim *Inorg. Chem.*, 47 (2008) 6289.
17. C. Garino, S. Ghiani, R. Gobetto C. Nervi, L. Salassa, E. Rosenberg, J. B. A. Ross X. Chu, K. I. Hardcastle, C. Sabatini *Inorg. Chem.* 46 (2007) 8752.
18. a) R. B. King *Inorg. Chem.* 2 (1963) 936. b) A. W. Verstuyft, J. H. Nelson, L. W. Cary *Inorg. Chem.* 15 (1976) 732. c) R. M. CatalaD. Cruz-Garriz, H. Torrens, R. L. Richards *J. Organometal. Chem.* 354 (1988) 123. d) J. T. Mague, S. E. Dessens *J. Organometal. Chem* 262 (1984) 347.
19. P. K. Maples, C. S. Kraihanzel *Chem. Commun* (1968) 922
20. M.L. Glbwka, D. Martynowski, K. Kozfowska *J of Molec. Struct.* 474 (1999) 81-89.

Synthesis, structure, photophysical and electrochemical properties of Ru(TFA)(CO)(PPh<sub>3</sub>)<sub>2</sub>(L) (L=2-phenylpyridine, 2-*p*-tolylpyridine) and Ru(CO)(PPhMe<sub>2</sub>)<sub>2</sub>(L)(L') (L= TFA, H) (L'= bipyridine, L'= 4,4'-dimethylbipyridine) relationships between ancillary ligand structure and luminescent properties

### Highlights

1. Two new Ru 2-ppy complexes with *trans*-PPh<sub>3</sub> have been synthesized and their physical and chemical properties are reported.
2. A series of Ru bpy complexes with *trans*-PPhMe<sub>2</sub> are also reported and the methyl groups all show the presence of strong virtual <sup>31</sup>P-<sup>31</sup>P virtual coupling.
3. The phenyl ring of the PPhMe<sub>2</sub> shows π-π stacking interactions with one of two phenyl rings of the bpy ligand.